Flexible Power Regulation and Current-limited Control of Grid-connected Inverter under Unbalanced Grid Voltage Faults

Guo, Xiaoqiang; Liu, Wenzhao; Lu, Zhigang

Published in:
IEEE Transactions on Industrial Electronics

Publication date:
2017

Document Version
Peer reviewed version

Flexible Power Regulation and Current-limited Control of Grid-connected Inverter under Unbalanced Grid Voltage Faults

Xiaoqiang Guo, *Senior Member*, *IEEE*, Wenzhao Liu, and Zhigang Lu

***Abstract*—The grid-connected inverters may experience excessive current stress in case of unbalanced grid voltage Fault Ride Through (FRT), which significantly affects the reliability of the power supply system. In order to solve the problem, the inherent mechanisms of the excessive current phenomenon with the conventional FRT solutions are discussed. The quantitative analysis of three phase current peak values are conducted and a novel current-limited control strategy is proposed to achieve the flexible active and reactive power regulation and successful FRT in a safe current operation area with the aim of improving the system reliability under grid faults. Finally, the simulation and experiments of traditional and proposed FRT solutions are carried out. The results verify the effectiveness of the proposed method.**

***Index Terms*—distributed generation; inverter; fault ride through, grid fault.**

I. INTRODUCTION

The distributed generation systems integrating renewable energy resources (RES) have attracted considerable attention due to the environmental aspects and flexible controllability [1-9]. In general, power electronic inverters which act as the interfaces between RESs and the grid should have the ability to enhance power quality and ride though the short-term disturbances or grid faults, especially under unbalanced grid conditions. The so called Fault Ride Through (FRT) capability [10-11] requires the grid-connected inverters to withstand grid voltage sags and remains connected to avoid sudden tripping and loss of power generation. The voltage collapse should be avoided by introducing flexible active and reactive power injection to support the grid voltage. Under these requirements, a wide range of FRT control strategies has been proposed to ensure the inverters operate flexibly under grid faults conditions.

The flexible power control concept, which facilitates multiple choices for FRT with different power/current references, has been proposed in [12-15]. An interesting FRT solution focused on the flexible power quality regulation by considering the instantaneous power ripples and current harmonics has been proposed in [16] where the current harmonic can be eliminated at the expense of active and reactive power oscillations. In [17], another FRT solution has been presented which is fully flexible since positive and negative sequence active and reactive power/current components can be simultaneously injected to improve the reliability of ride through services of grid-connected inverters. However, for three-phase three-wire grid-connected inverter systems, the control freedom seems not enough to eliminate instantaneous power oscillations and current harmonics at the same time from the viewpoint of classical instantaneous power theory [18]. An interesting control method which utilizes the zero sequence components is proposed in [19] to enhance flexible power controllability under unbalanced grid conditions. But the current reference generator is based on a six dimensional matrix, which increases the computational burden.

Furthermore, advanced control algorithms for FRT, which are mainly based on symmetric sequences to achieve particular control objectives related to the current harmonics, power oscillations, dc bus ripples and voltage support during the unbalanced grid voltage faults have been proposed in [20-22]. In fact, the excessive and harmonic current in case of the unbalanced grid FRT significantly affects the system operation reliability. The power oscillations may affect the continuity of power supply for inverter-based systems. However, few works have been developed for both flexible power controllability and peak current-limited capacity for grid-connected inverter especially under unbalanced grid faults. An interesting fault ride through control strategy is presented in [23]. The flexible power control can be achieved. But the current-limited issue is not discussed. In order to solve the problem, an insightful control strategy is reported in [24]. However, the method is complex to implement. Moreover, it depends on the voltage unbalance factor and phase angle between sequences, which limits its use in practical applications. Therefore, the simple but

Manuscript received July 15, 2015; revised September 7, 2016, and October 12, 2016; accepted October 22, 2016. This work was supported by the National Natural Science Foundation of China (51677161) and Science Foundation for Distinguished Young Scholars of Hebei Province (E2016203133).

X. Guo, W. Liu, and Z. Lu are with the Key Laboratory of Power Electronics for Energy Conservation and Motor Drive of Hebei Province, Department of Electrical Engineering, Yanshan University, Qinhuangdao 066004, China (e-mail: gxq@ysu.edu. cn).

This article has been accepted for publication in a future issue of this journal, but has not been fully edited. Content may change prior to final publication. Citation information: DOI 10.1109/TIE.2017.2669018, IEEE Transactions on Industrial Electronics

effective current-limited and flexible power control, which is independent of voltage unbalance factor and phase angle between sequences, needs further investigation.

In this paper, a novel current-limited control strategy is proposed to achieve the flexible power control and successful FRT within a safe current operation range under grid faults, which is beneficial to the reliability of power systems.

II. CONTROL STRATEGY

The schematic diagram of the grid-connected inverter is depicted in Fig. 1 [25]. Two modes, e.g. grid-connected and stand alone modes are operated in practice. In general, the voltage control is used in stand alone mode, while the current control can be used in grid connected mode. In this paper, the current controlled grid-connected mode is investigated, especially for the FRT control under unbalanced grid voltage faults condition.

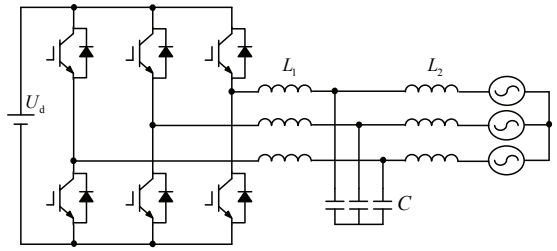

Fig.1. Schematic of grid-connected inverter

A. Quantitative analysis of overcurrent

Three-phase unbalanced grid voltage can be mathematically expressed as (1).

$$\begin{bmatrix} u_a \\ u_b \\ u_c \end{bmatrix} = \begin{bmatrix} U^+\sin(\omega t+\theta_p)+U^-\sin(\omega t+\theta_n) \\ U^+\sin(\omega t+\theta_p-120^\circ)+U^-\sin(\omega t+\theta_n+120^\circ) \\ U^+\sin(\omega t+\theta_p+120^\circ)+U^-\sin(\omega t+\theta_n-120^\circ) \end{bmatrix} \quad (1)$$

where U^+ and U^- are the voltage amplitude of positive and negative sequences. θ_p and θ_n are the phase angle of positive and negative sequences. ω is the angular frequency of the positive and negative sequences,

Three-phase unbalanced grid voltage can be expressed in stationary frame with the Clarke transformation.

$$\begin{cases} \begin{bmatrix} u_\alpha \\ u_\beta \end{bmatrix} = \frac{2}{3}\begin{bmatrix} 1 & -\frac{1}{2} & -\frac{1}{2} \\ 0 & \frac{\sqrt{3}}{2} & -\frac{\sqrt{3}}{2} \end{bmatrix}\begin{bmatrix} u_a \\ u_b \\ u_c \end{bmatrix} = \begin{bmatrix} u_\alpha^+ + u_\alpha^- \\ u_\beta^+ + u_\beta^- \end{bmatrix} \\ \begin{bmatrix} u_\alpha^+ \\ u_\beta^+ \end{bmatrix} = \begin{bmatrix} U^+\sin(\omega t+\theta_p) \\ -U^+\cos(\omega t+\theta_p) \end{bmatrix} \quad \begin{bmatrix} u_\alpha^- \\ u_\beta^- \end{bmatrix} = \begin{bmatrix} U^-\sin(\omega t+\theta_n) \\ U^-\cos(\omega t+\theta_n) \end{bmatrix} \end{cases} \quad (2)$$

With Instantaneous Power Theory, the active and reactive powers of the inverter can be obtained as:

$$\begin{bmatrix} p \\ q \end{bmatrix} = \frac{3}{2}\begin{bmatrix} u_\alpha & u_\beta \\ u_\beta & -u_\alpha \end{bmatrix}\begin{bmatrix} i_\alpha \\ i_\beta \end{bmatrix} \quad (3)$$

With (3), the inverter output current can be obtained as

$$\begin{bmatrix} i_\alpha \\ i_\beta \end{bmatrix} = \frac{2}{3}\begin{bmatrix} u_\alpha & u_\beta \\ u_\beta & -u_\alpha \end{bmatrix}^{-1}\begin{bmatrix} P^* \\ Q^* \end{bmatrix} = \begin{bmatrix} i_{\alpha(p)}+i_{\alpha(q)} \\ i_{\beta(p)}+i_{\beta(q)} \end{bmatrix} \quad (4)$$

where P^* and Q^* are the active and reactive power reference and detemined by the inverter rated capacity. $i_{\alpha(p)}, i_{\beta(p)}, i_{\alpha(q)}$ and $i_{\beta(q)}$ represent the active and reactive power current components in stationary frame respectively. Thus, equation (4) can be refermulated as follows

$$\begin{bmatrix} i_\alpha \\ i_\beta \end{bmatrix} = \begin{bmatrix} i_{\alpha(p)} \\ i_{\beta(p)} \end{bmatrix} + \begin{bmatrix} i_{\alpha(q)} \\ i_{\beta(q)} \end{bmatrix} = \frac{2}{3}\frac{P^*}{u_\alpha^2+u_\beta^2}\begin{bmatrix} u_\alpha \\ u_\beta \end{bmatrix} + \frac{2}{3}\frac{Q^*}{u_\alpha^2+u_\beta^2}\begin{bmatrix} u_\beta \\ -u_\alpha \end{bmatrix} \quad (5)$$

Substituting (2) into (5), the current components can be obtained as follows

$$\begin{cases} \begin{bmatrix} i_{\alpha(p)} \\ i_{\beta(p)} \end{bmatrix} = \frac{2}{3}\frac{P^*}{(u_\alpha^+ + u_\alpha^-)^2+(u_\beta^+ + u_\beta^-)^2}\begin{bmatrix} u_\alpha^+ + u_\alpha^- \\ u_\beta^+ + u_\beta^- \end{bmatrix} \\ \begin{bmatrix} i_{\alpha(q)} \\ i_{\beta(q)} \end{bmatrix} = \frac{2}{3}\frac{Q^*}{(u_\alpha^+ + u_\alpha^-)^2+(u_\beta^+ + u_\beta^-)^2}\begin{bmatrix} u_\beta^+ + u_\beta^- \\ -u_\alpha^+ - u_\alpha^- \end{bmatrix} \end{cases} \quad (6)$$

In order to realize the flexible power control during the FRT process, the adjustable coefficients k_p and k_q are introduced in (6) , and the inveter output current referenece can be rewritten as follows

$$\begin{cases} i_{\alpha(p)}^* = \frac{2}{3}\frac{P^*}{[(u_\alpha^+)^2+(u_\beta^+)^2]+k_p[(u_\alpha^-)^2+(u_\beta^-)^2]}[(u_\alpha^+)+(k_p u_\alpha^-)] \\ i_{\beta(p)}^* = \frac{2}{3}\frac{P^*}{[(u_\alpha^+)^2+(u_\beta^+)^2]+k_p[(u_\alpha^-)^2+(u_\beta^-)^2]}[(u_\beta^+)+(k_p u_\beta^-)] \\ i_{\alpha(q)}^* = \frac{2}{3}\frac{Q^*}{[(u_\alpha^+)^2+(u_\beta^+)^2]+k_q[(u_\alpha^-)^2+(u_\beta^-)^2]}[(u_\beta^+)+(k_q u_\beta^-)] \\ i_{\beta(q)}^* = \frac{2}{3}\frac{Q^*}{[(u_\alpha^+)^2+(u_\beta^+)^2]+k_q[(u_\alpha^-)^2+(u_\beta^-)^2]}[-(u_\alpha^+)-(k_q u_\alpha^-)] \end{cases} \quad (7)$$

It should be noted that k_p and k_q meet the requirement $k_p+k_q=0$. In particular, the special conditions of this control strategy for different applications can be divided into four modes as shown in Tab.I. However, all of these control targets lead to he excessive current stress, which significantly affects the operation reliability of power supply system.

TABLE I
TRADITIONAL FRT CONTROL MODES

Schemes	Control target	k_p	k_q
mode A	P remains constant	-1	1
mode B	Balanced sinusoidal current	0	0
mode C	Q remains constant	1	-1
mode D	P and Q flexible regulation	[-1,1]	[1,-1]

The following will present a quantitative analysis of inverter overcurrent. Substituting (2) into (7) and simplifying the equations to obtain the active and reactive power currents

This article has been accepted for publication in a future issue of this journal, but has not been fully edited. Content may change prior to final publication. Citation information: DOI 10.1109/TIE.2017.2669018, IEEE Transactions on Industrial Electronics

$$\begin{cases} I_{\alpha(p)}=\dfrac{2}{3}\dfrac{P^*}{[(U^+)^2+k_p(U^-)^2]}[U^+\sin(\omega t+\theta_p)+k_pU^-\sin(\omega t+\theta_n)] \\ I_{\beta(p)}=\dfrac{2}{3}\dfrac{P^*}{[(U^+)^2+k_p(U^-)^2]}[-U^+\cos(\omega t+\theta_p)+k_pU^-\cos(\omega t+\theta_n)] \\ I_{\alpha(q)}=\dfrac{2}{3}\dfrac{Q^*}{[(U^+)^2+k_q(U^-)^2]}[-U^+\cos(\omega t+\theta_p)+k_qU^-\cos(\omega t+\theta_n)] \\ I_{\beta(q)}=\dfrac{2}{3}\dfrac{Q^*}{[(U^+)^2+k_q(U^-)^2]}[-U^+\sin(\omega t+\theta_p)-k_qU^-\sin(\omega t+\theta_n)] \end{cases} \tag{8}$$

The inverter current reference in the stationary frame can be expressed as follows

$$\begin{aligned} \begin{bmatrix} I_\alpha^* \\ I_\beta^* \end{bmatrix} &= \begin{bmatrix} I_{\alpha(p)}+I_{\alpha(q)} \\ I_{\beta(p)}+I_{\beta(q)} \end{bmatrix} \\ &= \frac{2}{3}\begin{bmatrix} A_1\sin(\omega t+\theta_p-\delta_1)+A_2\sin(\omega t+\theta_n+\delta_2) \\ -A_1\cos(\omega t+\theta_p-\delta_1)+A_2\cos(\omega t+\theta_n+\delta_2) \end{bmatrix} \end{aligned} \tag{9}$$

where

$$A_1=\sqrt{[\frac{U^+P^*}{(U^+)^2+k_p(U^-)^2}]^2+[\frac{U^+Q^*}{(U^+)^2+k_q(U^-)^2}]^2},$$

$$\delta_1=\text{atan}\frac{Q^*[(U^+)^2+k_p(U^-)^2]}{P^*[(U^+)^2+k_q(U^-)^2]},$$

$$A_2=\sqrt{[\frac{k_pU^-P^*}{(U^+)^2+k_p(U^-)^2}]^2+[\frac{k_qU^-Q^*}{(U^+)^2+k_q(U^-)^2}]^2},$$

$$\delta_2=\text{atan}\frac{k_qQ^*[(U^+)^2+k_p(U^-)^2]}{k_pP^*[(U^+)^2+k_q(U^-)^2]}.$$

With the inverse Clarke transformation, equation (9) can be expressed in abc frame as follows

$$\begin{bmatrix} I_a^* \\ I_b^* \\ I_c^* \end{bmatrix}=\frac{2}{3}\begin{bmatrix} \sqrt{A_1^2+A_2^2-2A_1A_2\cos(\theta_p-\delta_1-\theta_n-\delta_2)}\sin(\omega t+\psi_a) \\ \sqrt{A_1^2+A_2^2-2A_1A_2\cos(\theta_p-\delta_1-\theta_n-\delta_2-240^\circ)}\sin(\omega t+\psi_b) \\ \sqrt{A_1^2+A_2^2-2A_1A_2\cos(\theta_p-\delta_1-\theta_n-\delta_2+240^\circ)}\sin(\omega t+\psi_c) \end{bmatrix} \tag{10}$$

where

$$\psi_a=\text{atan}\frac{A_1\sin(\theta_p-\delta_1)-A_2\sin(\theta_n+\delta_2)}{A_1\cos(\theta_p-\delta_1)-A_2\cos(\theta_n+\delta_2)},$$

$$\psi_b=\text{atan}\frac{A_1\sin(\theta_p-\delta_1-120^\circ)-A_2\sin(\theta_n+\delta_2+120^\circ)}{A_1\cos(\theta_p-\delta_1-120^\circ)-A_2\cos(\theta_n+\delta_2+120^\circ)},$$

$$\psi_c=\text{atan}\frac{A_1\sin(\theta_p-\delta_1+120^\circ)-A_2\sin(\theta_n+\delta_2-120^\circ)}{A_1\cos(\theta_p-\delta_1+120^\circ)-A_2\cos(\theta_n+\delta_2-120^\circ)}.$$

The peak value of the inverter output current can be obtained from (10) as follow

$$\begin{aligned} I_{\max}^* &= \frac{2}{3}\sqrt{A_1^2+A_2^2+2A_1A_2}=\frac{2}{3}(A_1+A_2) \\ &= \frac{2}{3}\sqrt{[\frac{U^+P^*}{(U^+)^2+k_p(U^-)^2}]^2+[\frac{U^+Q^*}{(U^+)^2+k_q(U^-)^2}]^2} \\ &+\frac{2}{3}\sqrt{[\frac{k_pU^-P^*}{(U^+)^2+k_p(U^-)^2}]^2+[\frac{k_qU^-Q^*}{(U^+)^2+k_q(U^-)^2}]^2} \end{aligned} \tag{11}$$

Thus, the current peak value can be estimated which is beneficial to the traditional FRT control protection. On the other hand, if the grid voltage is balanced which means negative sequence voltage U^-=0, three phase inverter output current peak values are expressed as (12)

$$I_{\text{max-balance}}^*=\frac{2\sqrt{(P^*)^2+(Q^*)^2}}{3U^+}=\frac{2S}{3U^+} \tag{12}$$

From equations (11) and (12), it can be observed that the inverter current peak values are only determined by grid positive voltage U^+ and apparent power parameter S under normal grid voltage conditions. However, it is more complex to minimize the inverter current peak values under the unbalanced grid faults because of this fact that the current peak value is not only determined by the coupled active/reactive powers/currents but also by positive/negative sequence grid voltage components. In such cases, the injection of positive and negative sequence powers will inherently induce different amplitudes of three phase inverter output current and affect the reliability of power system. Quantitative computation results of inverter current are shown in Tab. II with the system parameters in Tab. IV.

TABLE II
OPERATING STATES AND CURRENT PEAK VALUES

States	Adjust coefficient	Current peak value
normal	$k_p, k_q \in$ [-1,1]	5.0 A
unbalanced	$k_p=-1$, $k_q=1$	8.7 A
	$k_p=-0.5$, $k_q=0.5$	7.6 A
	$k_p=0$, $k_q=0$	6.5 A
	$k_p=0.5$, $k_q=-0.5$	7.4 A
	$k_p=1$, $k_q=-1$	8.3 A

Furthermore, in order to achieve unity power factor and constant active power output, the reactive power can be set as Q^* =0 and k_p=-1 which is also the highest peak current condition. Thus, the current peak value under normal and unbalanced grid voltage conditions can be expressed as (13) and (14) respectively

$$I_{\text{balanced-P}}^*=\frac{2P^*}{3U^+} \tag{13}$$

$$I_{\text{unbalanced-P}}^*=\frac{2P^*}{3(U^+-U^-)} \tag{14}$$

From equations (13) and (14), it can be observed that the inverter current peak values under unbalanced conditions are always higher than normal conditions because of the negative

sequence voltage component U^-. Therefore, FRT solutions which focus on the minimized peak current control are attractive. The following subsection presents a solution for grid-connected inverters to ensure current-limited operation.

B. Proposed control strategy

Based on the above analysis, the inverter current will increase under the unbalanced grid faults to keep the power reference P^* and Q^* constant. Alternatively, the power reference can be approximately calculated by the product of current references and positive grid voltage. Thus, the inverter output current can be obtained as follows

$$\begin{cases} i^*_{\alpha(p)} = \dfrac{2}{3}\dfrac{I^*_p\sqrt{(u^+_\alpha)^2+(u^+_\beta)^2}}{[(u^+_\alpha)^2+(u^+_\beta)^2]+k_p[(u^-_\alpha)^2+(u^-_\beta)^2]}[(u^+_\alpha)+(k_p u^-_\alpha)] \\ i^*_{\beta(p)} = \dfrac{2}{3}\dfrac{I^*_p\sqrt{(u^+_\alpha)^2+(u^+_\beta)^2}}{[(u^+_\alpha)^2+(u^+_\beta)^2]+k_p[(u^-_\alpha)^2+(u^-_\beta)^2]}[(u^+_\beta)+(k_p u^-_\beta)] \\ i^*_{\alpha(q)} = \dfrac{2}{3}\dfrac{I^*_q\sqrt{(u^+_\alpha)^2+(u^+_\beta)^2}}{[(u^+_\alpha)^2+(u^+_\beta)^2]+k_q[(u^-_\alpha)^2+(u^-_\beta)^2]}[(u^+_\beta)+(k_q u^-_\beta)] \\ i^*_{\beta(q)} = \dfrac{2}{3}\dfrac{I^*_q\sqrt{(u^+_\alpha)^2+(u^+_\beta)^2}}{[(u^+_\alpha)^2+(u^+_\beta)^2]+k_q[(u^-_\alpha)^2+(u^-_\beta)^2]}[-(u^+_\alpha)-(k_q u^-_\alpha)] \end{cases} \tag{15}$$

where I^*_p *and* I^*_q represent the active and reactive current references, respectively.

It should be noted that the average value of the injected active or reactive power over one grid cycle only matches the reference active or reactive power for some particular values of k_p, and k_q. The reason is that the current limitation function is the first priority under grid faults. Otherwise, the over-current phenomenon would occur if the average value of the injected power matches the reference power. So in order to avoid the over-current phenomenon, the average value of the injected active or reactive power might be slightly smaller than its reference. It should be noted that the grid fault generally occurs and then cleared within a short interval. So this slight power mismatch is acceptable in practical application.

The peak values of three phase grid-connected inverter output current can be obtained from (15) as follow

$$I^*_{\max} = \frac{2}{3}\sqrt{\left[\frac{I^*_p(U^+)^2}{(U^+)^2+k_p(U^-)^2}\right]^2+\left[\frac{I^*_q(U^+)^2}{(U^+)^2+k_q(U^-)^2}\right]^2} + \frac{2}{3}\sqrt{\left[\frac{k_p I^*_p U^+U^-}{(U^+)^2+k_p(U^-)^2}\right]^2+\left[\frac{k_q I^*_q U^+U^-}{(U^+)^2+k_q(U^-)^2}\right]^2} \tag{16}$$

With the same system parameters of Table IV, the quantitative computation results of inverter current in (16) under normal and unbalanced grid conditions are shown in Table III.

Compared with the conventional FRT solution, the proposed method can reduce the peak values under unbalanced grid fault from 8.7A (c.f Tab. II) to 6.7A (c.f Tab. III) But, the current peak values are still beyond 5A, which corresponds to rated current.

TABLE III
OPERATING STATES AND CURRENT PEAK VALUES

States	Adjust coefficient	Current peak value
normal	$k_p, k_q \in$ [-1,1]	5.0 A
unbalanced	$k_p=-1$, $k_q=1$	6.7 A
	$k_p=-0.5$, $k_q=0.5$	5.8 A
	$k_p=0$, $k_q=0$	5.0 A
	$k_p=0.5$, $k_q=-0.5$	5.7 A
	$k_p=1$, $k_q=-1$	6.4 A

Further, In order to keep the current within a safe operation range, the grid-connected inverter should be equipped with current-limited capacity. The overall control structure is shown in Fig. 2.

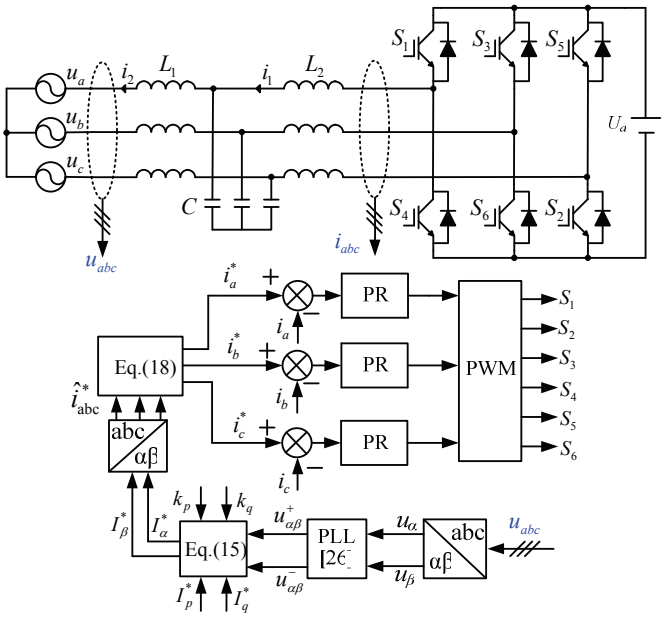

Fig.2. Control structure of the proposed current-limited strategy

In Fig. 2, the MCCF-PLL is used for estimating the positive and negative sequences of grid voltage [26]. Other PLL can also be utilized for grid synchronization [27-29]. The three-phase current is independently controlled by three Proportional-Resonant (PR) controllers with a single current-loop control. R_d is used to damp the potential resonance from LCL filter. Other filters can also be used in practice [30-31]. Note that the current-limited reference generator operates in abc frame which is beneficial due to the convenience of actual current peak detection and comparison in real time.

Based on the analysis in (16), the current peak value is mainly determined by current references I^*_p *and* I^*_q and the positive/negative sequence grid voltage. Substituting the current reference (15) into the Clarke transformation, the actual three phase currents can be derived as

This article has been accepted for publication in a future issue of this journal, but has not been fully edited. Content may change prior to final publication. Citation information: DOI 10.1109/TIE.2017.2669018, IEEE Transactions on Industrial Electronics

$$\begin{bmatrix} \hat{i}_a^* \\ \hat{i}_b^* \\ \hat{i}_c^* \end{bmatrix} = \begin{bmatrix} i_{\alpha(p)}^* + i_{\alpha(q)}^* \\ -(i_{\alpha(p)}^* + i_{\alpha(q)}^*)/2 + \sqrt{3}(i_{\beta(p)}^* + i_{\beta(q)}^*)/2 \\ -(i_{\alpha(p)}^* + i_{\alpha(q)}^*)/2 - \sqrt{3}(i_{\beta(p)}^* + i_{\beta(q)}^*)/2 \end{bmatrix} \quad (17)$$

In order to limit the current within an acceptable level during grid faults, the current references in (17) is modified, as shown in (18), where I_{rated} represents the rated current value of the inverter, I_{max} represents the maximum current value in three phase output currents, that is, $I_{\max} = \max(\hat{i}_a^*, \hat{i}_b^*, \hat{i}_c^*)$.

$$\begin{bmatrix} \hat{i}_a^* \\ \hat{i}_b^* \\ \hat{i}_c^* \end{bmatrix} = \frac{I_{rated}}{I_{\max}} \begin{bmatrix} \hat{i}_a^* \\ \hat{i}_b^* \\ \hat{i}_c^* \end{bmatrix} = \frac{I_{rated}}{I_{\max}} \begin{bmatrix} \hat{i}_{\alpha(p)}^* + \hat{i}_{\alpha(q)}^* \\ -(\hat{i}_{\alpha(p)}^* + \hat{i}_{\alpha(q)}^*)/2 + \sqrt{3}(\hat{i}_{\beta(p)}^* + \hat{i}_{\beta(q)}^*)/2 \\ -(\hat{i}_{\alpha(p)}^* + \hat{i}_{\alpha(q)}^*)/2 - \sqrt{3}(\hat{i}_{\beta(p)}^* + \hat{i}_{\beta(q)}^*)/2 \end{bmatrix} \quad (18)$$

It is clear that the current reference peak value in equation (18) will not go beyond I_{rated} under the unbalanced grid voltage conditions.

Compared with the conventional method in [24], which is very complex and depends on the voltage unbalance factor and phase angle between sequences, the proposed current-limited method is independent on the voltage unbalance factor and phase angle between sequences. Therefore, it is simple to implement in practice. Other details can be found in our granted patent [32].

III. Simulation and Experimental Results

In this section, the proposed control strategy is verified by simulation and experimental tests. The time-domain simulation with MATLAB and hardware-based experiments are conducted by comparing the conventional and proposed current-limited FRT control strategy. The test parameters are listed in Table IV.

TABLE IV
System Parameters

parameters	value	parameters	value
u_{dc}/V	120	u_a/V	50∠ 0°
u_b/V	34.2∠ –137°	u_c/V	34.2∠ 137°
U^+/V	38.5	U^-/V	11.5
P^*/W	300	Q^*/var	225
I_p^*/A	6	I_q^*/A	4.5
L_1/mH	5	L_2/mH	1
C/μF	9.9	R_d/Ω	5
k_p	0.15	k_r	20

A. Simulation results

Fig. 3 shows the simulation results of the conventional control strategy. Before the grid fault, the grid current is 5A as the rated value. However, the current tends to be much higher after the grid fault. As the coefficient of k_p varies, the active and reactive powers can be flexibly regulated. The current is beyond the rated value of 5A all the time.

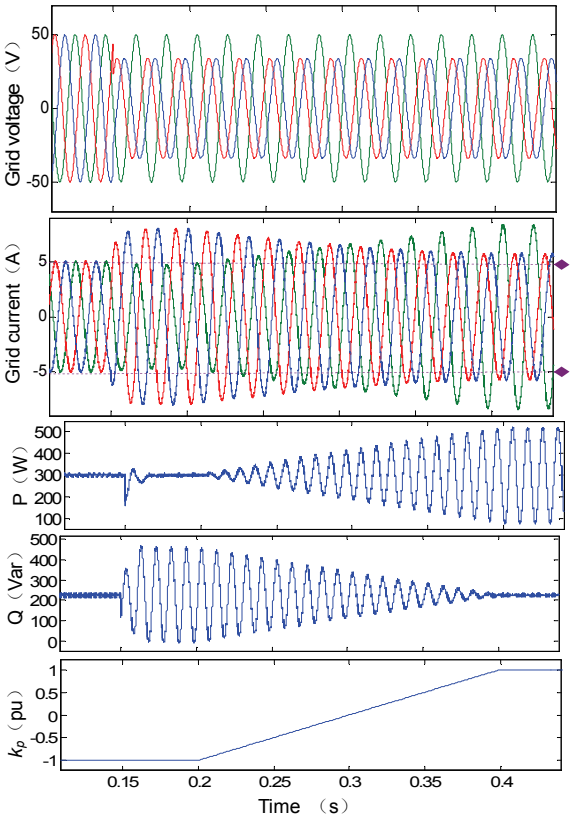

Fig. 3 Simulation results of conventional control strategy

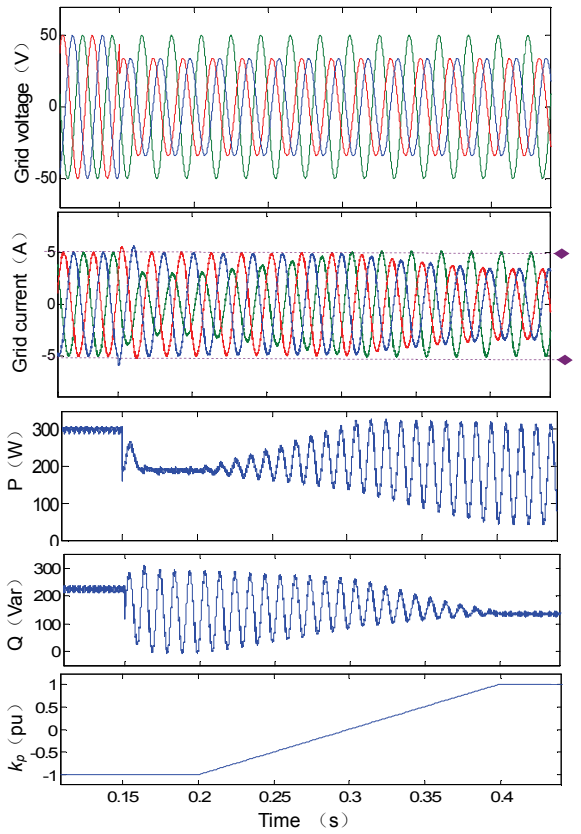

Fig. 4 Simulation results of proposed control strategy

This article has been accepted for publication in a future issue of this journal, but has not been fully edited. Content may change prior to final publication. Citation information: DOI 10.1109/TIE.2017.2669018, IEEE Transactions on Industrial Electronics

Fig. 4 shows the simulation results of the proposed control strategy. After the grid fault, the active and reactive powers can be flexibly adjusted as the coefficient of k_p varies. Moreover, the current is well regulated, and the peak value is not beyond the rating of 5A after the grid faults.

B. Experiment Results

In order to further verify the effectiveness of the proposed solution, the hardware experimental platform is built in the lab. a Chroma 62050H-600 DC programmable source is used for mimicking the renewable energy sources. The grid fault is emulated by the Chroma 6590 programmable AC source. A 32-bit fixed-point 150MHz TMS320F2812 DSP is used to control the inverter. The experimental results are provided as follows.

Fig. 5 shows the experimental results of the conventional control strategy with increasing adjustable coefficient k_p changed from -1 to 1. It is can be observed that the peak value of the grid current is far beyond the rating of 5A after the grid faults. The maximum value is in agreement with the theoretical calculation results in Tab. II. On the other hand, the active and reactive powers can be flexibly regulated for some specific microgrid applications which are sensitive to power oscillations.

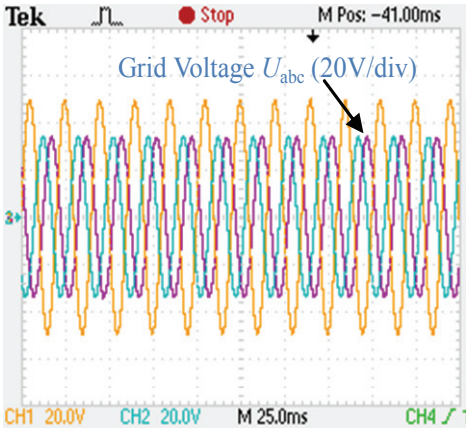

(a)

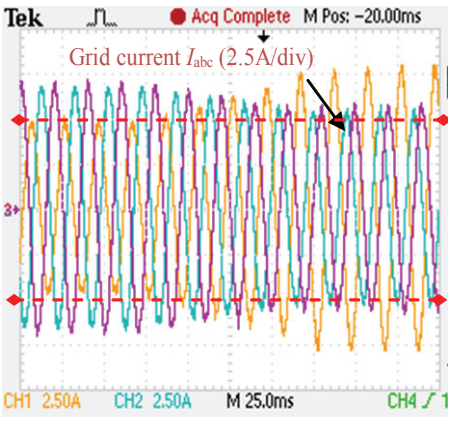

(b)

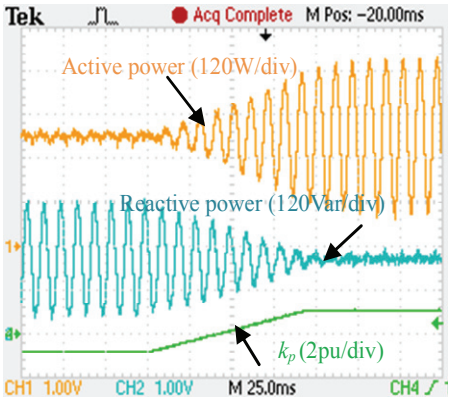

(c)

Fig. 5 Experimental results of conventional control strategy.

Fig. 6 shows the experimental results of the proposed control strategy. It can be observed that the active and reactive powers can be regulated in a flexible way. Furthermore, the grid current can be well controlled with the proposed current-limited solution, which avoids the over-current phenomenon under the grid faults.

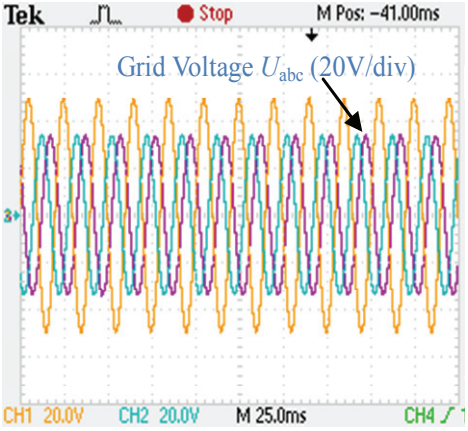

(a)

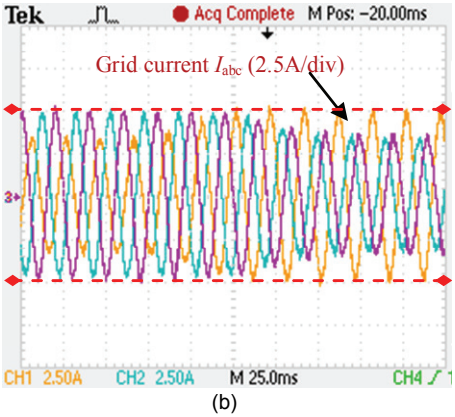

(b)

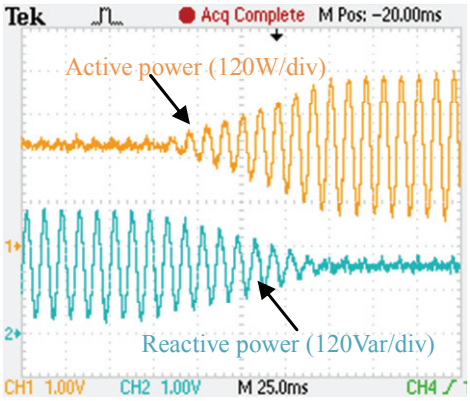

(c)

Fig. 6 Experimental results of proposed control strategy.

IV. Conclusion

This paper has presented the theoretical analysis and experimental verification of a new FRT control strategy for grid-connected inverters. Our findings indicate that the conventional FRT control method results in the over-current phenomenon, which degrades the system reliability. By replacing the power reference with current one, the peak current can be reduced, but still beyond the rated value. With the proposed method, the peak current can be effectively controlled within the rated value. Meanwhile, the flexible power control can be achieved. The experimental results verify the effectiveness of the proposed solution.

Reference

[1] X. Guo, and X. Jia, "Hardware-based cascaded topology and modulation strategy with leakage current reduction for transformerless PV systems," *IEEE Trans. Ind. Electron*., vol. 62, no. 12, pp. 7823–7832, Dec. 2016.

[2] J. Hu, L. Sun, X. Yuan, S. Wang, and Y. Chi. Modeling of type 3 wind turbine with df/dt inertia control for system frequency response study," *IEEE Trans. Power Syst.* DOI: 10.1109/TPWRS.2016.2615631.

[3] X. Guo, "A novel CH5 inverter for single-phase transformerless photovoltaic system applications," *IEEE Trans. Circuits and Systems I: Express Briefs*, in press, 2016.

[4] Z. Shao, X. Zhang, F. Wang, R. Cao, and H. Ni, "Analysis and control of neutral-point voltage for transformerless three-level PV inverter in LVRT operation," *IEEE Trans. Power Electron*., vol. 32, no. 3, pp. 2347 –2359, Mar. 2017.

[5] X. Guo, *et al*, "Leakage current suppression of three phase flying capacitor PV inverter with new carrier modulation and logic function," *IEEE Trans. Power Electron*., In press, 2016

[6] H. Geng, C. Liu, and G. Yang. "LVRT capability of DFIG based WECS under asymmetrical grid fault condition," *IEEE Trans. Ind. Electron*., vol. 60, no. 6, pp. 2495-2509, Jun. 2013.

[7] X. Guo, *et al*, "Three phase ZVR topology and modulation strategy for transformerless PV system," *IEEE Trans. Power Electron*., in press 2016.

[8] W. Li, Y. Gu, H. Luo, W. Cui, X. He, and C. Xia, "Topology review and derivation methodology of single-phase transformerless photovoltaic inverters for leakage current suppression," *IEEE Trans. Ind. Electron*., vol. 62, no. 7, pp. 4537–4551, Jul. 2015.

[9] X. Guo, *et al*, "Transformerless Z-Source four-leg PV Inverter with leakage current reduction," *IEEE Trans. Power Electron*., In press, 2016

[10] J. Hu, Bo Wang, W. Wang, H. Tang, Y. Chi, and Q. Hu. "Small signal dynamics of DFIG-based wind turbines during riding through symmetrical faults in weak ac grid., *IEEE Trans. Energy Conv.,* DOI: 10.1109/TEC.2017.2655540.

[11] H. Nian, P. Cheng, Z. Zhu, "Independent operation of DFIG-based WECS using resonant feedback compensators under unbalanced grid voltage conditions", *IEEE Trans. Power Electron*., vol.30, no.7, pp.3650-3661, Jul. 2015

[12] Y. Zhang and C. Qu, "Model predictive direct power control of PWM rectifier under unbalanced network conditions," *IEEE Trans. Ind. Electron*., vol. 62, no. 7, pp. 4011-4022, 2015.

[13] Y. Zhang and C. Qu, "Direct power control of a pulse width modulation rectifier using space vector modulation under unbalanced grid voltages," *IEEE Trans. Power Electron*., vol. 30, no. 10, pp. 5892-5901, 2015.

[14] Rodriguez, P., Timbus, A. V., Teodorescu, R., Flexible active power control of distributed power generation systems during grid faults. *IEEE Trans .Ind. Electron.*, vol,54, no. 5, pp. 2583–2592, 2007.

[15] Z. Xie, X. Zhang, X. Zhang, S. Yang and L. Wang, "Improved ride-through control of dfig during grid voltage swell," *IEEE Trans. Ind. Electron*., vol. 62, no. 6, pp. 3584-3594, Jun. 2015.

[16] Guo X, Liu W, Zhang X, et al. "Flexible control strategy for grid-connected inverter under unbalanced grid faults without PLL." *IEEE Trans. Power Electron.*, vol. 30,no.4, pp. 1773–1778, 2015.

[17] T. Lee, S. Hu, and Y. Chan, "D-STATCOM with positive-sequence admittance and negative-sequence conductance to mitigate voltage fluctuations in high-level penetration of distributed generation systems," *IEEE Trans. Ind. Electron.*, vol. 60, no. 4, pp. 1417–1428, 2013.

[18] W. Jiang, Y. Hu, Y. Zhang, D. Zhao, and L. Wang , "Different control objectives for grid-connected converter under unbalanced grid voltage using forgotten iterative filter as phase lock loop." *IET Trans. Power Electron.*, vol. 8,no.9, pp. 1798–1807, 2015.

[19] Ma, K., Chen, W., Liserre, M., and Blaabjerg, F. "Power controllability of a three-phase converter with an unbalanced AC source," *IEEE Trans. Power Electron*, vol.30, no. 3, pp 1591-1604. 2015.

[20] K. Sun, X. Wang, Y. Li, F. Nejabatkhah, Y. Mei, and X. Lu, "Parallel operation of bidirectional interfacing converters in a hybrid AC/DC microgrid under unbalanced grid voltage conditions," *IEEE Trans. Power Electron*., vol. 32, no. 3, pp. 1872-1884, 2017.

[21] X. Guo, X. Zhang, B. Wang, W. Wu, and J. Guerrero, "Asymmetrical grid fault ride-through strategy of three-phase grid-connected inverter considering network impedance impact in low-voltage grid," *IEEE Trans. Power Electron*., vol. 29, no. 3, pp. 1064–1068, Mar. 2014.

[22] H. Nian, Y. Shen, H. Yang, and Y. Quan, "Flexible grid connection technique of voltage-source inverter under unbalanced grid conditions based on direct power control," *IEEE Trans. Ind. Appl*., vol. 51, no. 5, pp. 4041–4050, 2015.

[23] F. Wang, J. L. Duarte, and M. A. M. Hendrix, "Pliant active and reactive power control for grid-interactive converters under unbalanced voltage dips," *IEEE Trans. Power Electron*., vol. 26, no. 5, pp. 1511–1521, 2011.

[24] Camacho, Antonio, et al. "Active and reactive power strategies with peak current limitation for distributed generation inverters during unbalanced grid faults *IEEE Trans. Ind. Electron.*, vol. 62, no. 3, pp.1515-1525,.2015.

[25] X. Guo, *et al*, "Abc-frame complex-coefficient filter and controller based current harmonic elimination strategy for three-phase grid connected inverter," *J. Mod. Power Syst. Clean Energy*, vol. 4, no. 1, pp. 87–93, Jan. 2016.

[26] X. Guo, W. Wu, and Z. Chen, "Multiple-complex coefficient-filter-based phase-locked loop and synchronization technique for three-phase grid interfaced converters in distributed utility networks," *IEEE Trans. Ind. Electron*., vol. 58, no. 4, pp. 1194–1204, Apr. 2011.

[27] L. Zheng, H. Geng, and G. Yang. "Fast and robust phase estimation algorithm for heavily distorted grid conditions," *IEEE Trans. Ind. Electron*., vol. 63, no. 11, pp. 6845–6855, Nov. 2016.

[28] F. Wu, D. Sun, L. Zhang, and J. Duan, "Influence of plugging DC offset estimation integrator in single-phase EPLL and alternative scheme to eliminate effect of input DC offset and harmonics," *IEEE Trans. Ind. Electron*., vol. 62, no. 8, pp. 4823-4831, Aug. 2015.

[29] F. Wu, L. Zhang, and J. Duan, "A new two-phase stationary frame based enhanced PLL for three-phase grid synchronization," *IEEE Trans. Circuits and Systems—II: Express Briefs*, vol. 62, no. 3, pp. 251-255, Mar. 2015.

[30] W. Wu, M. Huang, X. Wang, H. Wang, F. Blaabjerg, M. Liserre, and H. S. Chung, "A robust passive damping method for LLCL-filter-based grid-tied inverters to minimize the effect of grid harmonic voltages," *IEEE Trans. Power Electron*., vol. 29, no. 7, pp. 3279–3289, Jul. 2014.

[31] W. Wu, Y. He, and F. Blaabjerg, "A new design method for the passive damped LCL- and LLCL-filter based single-phase grid-tied inverter," *IEEE Trans. Ind. Electron*., vol. 60, no. 10, pp. 4339–4350, Oct. 2013.

[32] X. Guo, *et al*, "A control method for fault ride through of grid-connected PV inverter," Patent, ZL 201410131069.8, 2014

X. Guo (M' 10-SM' 14) received the B.S. and Ph.D. degrees in electrical engineering from Yanshan University, Qinhuangdao, China, in 2003 and 2009, respectively.

He has been a Postdoctoral Fellow with the Laboratory for Electrical Drive Applications and Research (LEDAR), Ryerson University, Toronto, ON, Canada. He is currently an associate professor with the Department of Electrical Engineering, Yanshan University, China. He has authored/coauthored more than sixty technical papers, in addition to nine patents. His current research interests include high-power converters and ac drives, electric vehicle charging station, and renewable energy power conversion systems.

Dr. Guo is a Senior Member of the IEEE Power Electronics Society and IEEE Industrial Electronics Society. He is an active Referee for IEEE Transactions on Industrial Electronics and IEEE Transactions on Power Electronics.

W. Liu received the B.S. and M.S. degrees in electrical engineering and power electronics from Yanshan University, Qinhuangdao, China, in 2012 and 2015, respectively. He is currently working toward the Ph.D. degree in power electronics at Aalborg University, Aalborg, Denmark. His research interests include control of power electronic converters for renewable energy systems.

Z. Lu received the B.S. degree in automatic control and the M.S. degree in systems engineering from Xi'an Jiaotong University, Xi'an, China, in 1985 and 1988, respectively, and the Ph.D. degree in electric power systems and automation from the North China Electric Power University, Beijing, China, in 1998. His current research interests include operation and control of power systems, power grid state estimation, power system planning, and renewable energy power conversion systems.